



HAL
open science

Indirect Pockels effect in rubidium hydrogen selenate

Laurent Guilbert, Jean-Paul Salvestrini, Z. Czapla

► **To cite this version:**

Laurent Guilbert, Jean-Paul Salvestrini, Z. Czapla. Indirect Pockels effect in rubidium hydrogen selenate: measurement of the large r_{42} coefficient. *Journal of the Optical Society of America B*, 2000, 17 (12), pp.1980-1985. 10.1364/JOSAB.17.001980 . hal-00186033

HAL Id: hal-00186033

<https://hal.science/hal-00186033>

Submitted on 3 Dec 2021

HAL is a multi-disciplinary open access archive for the deposit and dissemination of scientific research documents, whether they are published or not. The documents may come from teaching and research institutions in France or abroad, or from public or private research centers.

L'archive ouverte pluridisciplinaire **HAL**, est destinée au dépôt et à la diffusion de documents scientifiques de niveau recherche, publiés ou non, émanant des établissements d'enseignement et de recherche français ou étrangers, des laboratoires publics ou privés.



Distributed under a Creative Commons Attribution - NonCommercial 4.0 International License

Indirect Pockels effect in rubidium hydrogen selenate: measurement of the larger r_{42} coefficient

Laurent Guilbert and J. P. Salvestrini

Laboratoire Matériaux Optiques, Photonique et Systèmes, Centre Lorrain d'Optique et d'Electronique des Solides, Université de Metz et Supelec 2, rue Edouard Belin, 57070 Metz Cedex, France

Z. Czapla

Institute of Experimental Physics, University of Wrocław, Place Maxa Born'a 9, 50-205 Wrocław, Poland

The frequency dispersion of the large electro-optic effect in rubidium hydrogen selenate is measured from 300 Hz to 200 kHz as a function of the direction of propagation. It is shown that the major coefficient is r_{42} (750 pm/V at 1 kHz). Both dielectric and electro-optic responses exhibit strong, perfectly correlated dispersions in this frequency range. The experimental results confirm the major contribution of domain dynamics in the huge electro-optic effect and are in perfect agreement with calculations based on the tilting of the optical indicatrix. The possible use of rubidium hydrogen selenate in low-frequency electro-optic modulators is briefly discussed.

1. INTRODUCTION

A few years ago we found a strong Pockels effect in rubidium hydrogen selenate (RHSe) at low frequency.¹ Experimental results obtained so far have suggested that the large electro-optic (EO) properties of RHSe were related to domain dynamics. First, it was shown that the EO effect was strongly enhanced when the light beam was propagating at a large angle from the c axis perpendicular to domain walls.² This effect was also very sensitive to the dc bias superimposed on the ac voltage applied to the sample. Furthermore, the field-induced birefringence exhibited hysteresis cycles similar to that of the ferroelectric polarization, except when the light was propagated exactly along the c axis, and the frequency dispersions of both EO and dielectric responses were strongly correlated.³ As far as the domain dynamics contribution prevails, mainly r_{42} and r_{52} coefficients should be involved in the indirect Pockels effect, because in the ferroelectric–ferroelastic phase of RHSe (Aizu's species $2F1$) the main components of the order parameters are P_2 (ferroelectric polarization along the x_2 axis), e_4 , and e_5 (ferroelastic shear strains from monoclinic to triclinic structure).

The present work definitely confirms that the large EO properties of RHSe are related to domain dynamics. The variations of the effective EO coefficient $n^3 r_{\text{eff}}$ are accurately measured versus both the propagation direction and the frequency. The results show that $n^3 r_{\text{eff}}$ is proportional to $\sin 2i$ (i angle of incidence of the light beam with respect to the axis normal to the domain walls) and to the modulus of the complex dielectric susceptibility χ_d related to domain dynamics. By this method the r_{42} coefficient can be determined accurately. On the other hand, the contribution of domain dynamics to the r_{42} coefficient can be theoretically related to the product

$\chi_d \times \Delta n_1 \times \sin 2\phi_1$, where Δn_1 is the birefringence and $2\phi_1$ is the mutual tilt angle of the neutral lines in neighboring domains as seen from the x_1 axis. Experimental results are fully consistent with this theoretical expression. The same considerations can apply for the r_{52} coefficient, which has not been measured here, but which can be estimated to be $\sim 7\%$ of r_{42} .

2. EXPERIMENT

A. Sample Preparation

A parallelepipedic sample is cut perpendicular to the pseudo-orthorhombic axes from a pure solution-grown RHSe crystal. The corresponding dimensions along a , b , and c are 3.7, 4.5, and 3.0 mm, respectively. After polishing, gold electrodes are evaporated on the b -cut faces in order to apply the electric field along the ferroelectric axis. The sample is placed in a specific cell allowing accurate optical orientation in the laser beam and free rotation around the vertical axis (Fig. 1). Thin copper wires are connected to the gold electrodes with silver paste, threaded through a tubular rod outside the cell, and plugged to an electrical supply. The cell is filled with silicon oil (refractive index of 1.403) to reduce the refraction at large angles of incidence and to protect the crystal from humidity during experiments.

B. Definition of the Pseudoprincipal Axes

Since the ferroelectric–ferroelastic domain structure of RHSe consists of a single set of walls parallel to the crystal plane (001), the optical indicatrices in neighboring domains are tilted symmetrically with respect to the plane of the domain walls. To describe the optical and electro-

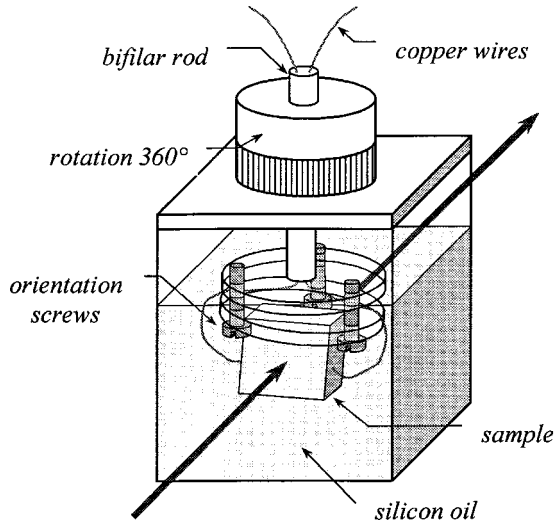


Fig. 1. Rotating sample holder for electro-optic measurements versus incidence angle.

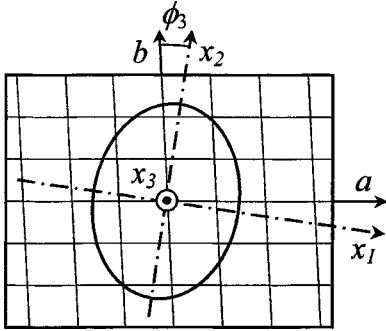


Fig. 2. Definition of the pseudoprincipal axes in the pseudomonoclinic crystal system: x_3 is perpendicular to the plan of W-domain walls; x_1 and x_2 are the neutral lines in this plane.

optical properties of polydomain RHSe, the convenient orthogonal axes are the so-called pseudoprincipal axes⁴ defined as follows (Fig. 2):

x_3 ($\equiv c$) is the axis perpendicular to the crystalline plane (a , b) of domain walls;

x_1 , x_2 are optical neutral lines (fast and slow, respectively) in the wave plane (a , b).

These axes can be considered, on average, as principal axes in the pseudomonoclinic structure of the polydomain sample. (They should become true principal axes in the paraelastic phase, above $T_C = 97^\circ\text{C}$). The corresponding pseudoprincipal refractive indices along these axes are noted n_1 , n_2 , and n_3 . The corresponding pseudoprincipal birefringences in the perpendicular wave planes are noted Δn_1 , Δn_2 , and Δn_3 . The tilt angle of the neutral lines in one given domain (plus or minus sign) with respect to the plane of the domain wall (Fig. 3) is noted $\pm\phi_1$ in the wave plane (x_2 , x_3) and $\pm\phi_2$ in the wave plane (x_3 , x_1). All these optical parameters have been measured for different wavelengths and reported in Ref. 4. They are recalled in Table 1 for the wavelength 633 nm. Note that the pseudoprincipal parameters are not very different from the true principal parameters, since the tilt angles ϕ_1 and ϕ_2 are small. Note also that

ϕ_3 is small, too. So in Fig. 2 the axes x_1 and x_2 are close to the crystal axes a and b . In the following, the propagation direction of the laser beam will always be defined with respect to the pseudoprincipal axes.

C. Birefringence and Electro-Optic Measurements

EO measurements are made in a Sénarmont setup (Fig. 4) with a He-Ne laser at the wavelength 633 nm. One of the a -cut faces of the crystal is glued by wax on the sample holder of the cell (as in Fig. 1). Then with the orientation screws of the sample holder, the crystal is oriented carefully so that the x_1 axis becomes parallel to the rotation axis of the cell. This parallelism is achieved by rotating the sample holder between crossed polarizers and checking the extinction of the laser beam. This configuration allows us to study the field-induced birefringence and the EO response versus the direction of propagation in the pseudoprincipal plane (x_2 , x_3). The sample

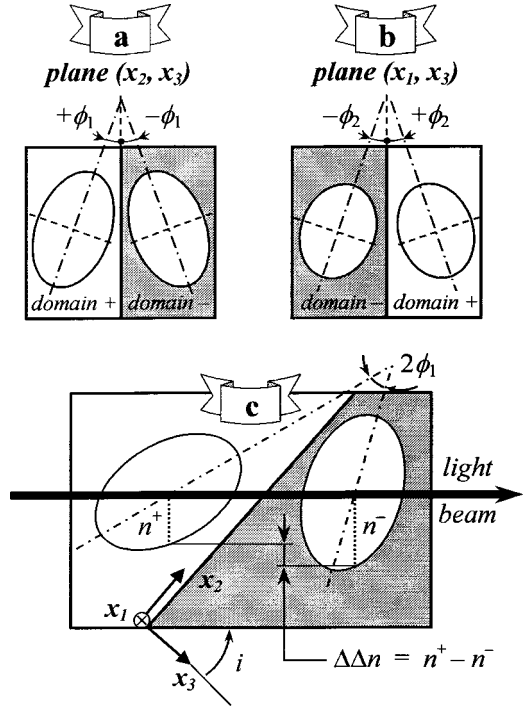


Fig. 3. Tilt of the optical indicatrix as seen from axes (a) x_1 and (b) x_2 . For clarity the small values of the tilt angles ($\phi_1 = -2.2^\circ$ and $\phi_2 = 0.6^\circ$) are voluntarily increased. (c) The variation of the extraordinary index n from domain to domain when the light beam is propagated in the plane (x_2 , x_3) is shown schematically. The other index is quasiordinary and keeps practically the same value ($\approx n_1$) in both types of domains.

Table 1. Optical Parameters^a of RHSe at 633 nm in the Ferroelastic Phase, 293 K^b

Pseudoprincipal Indices	Pseudoprincipal Birefringences	Tilt Angles of the Neutral Lines
$n_1 = 1.521(1)$	$\Delta n_1 = 0.0560(4)$	$\phi_1 = -2.2(1)^\circ$
$n_2 = 1.563(1)$	$\Delta n_2 = 0.0139(4)$	$\phi_2 = +0.6(2)^\circ$
$n_3 = 1.507(1)$	$\Delta n_3 = 0.0421(6)$	$\phi_3 = -6.0(3)^\circ$

^aThese data refer to the so-called pseudoprincipal axes, as defined in Figs. 2 and 3.

^bFrom Ref. 4.

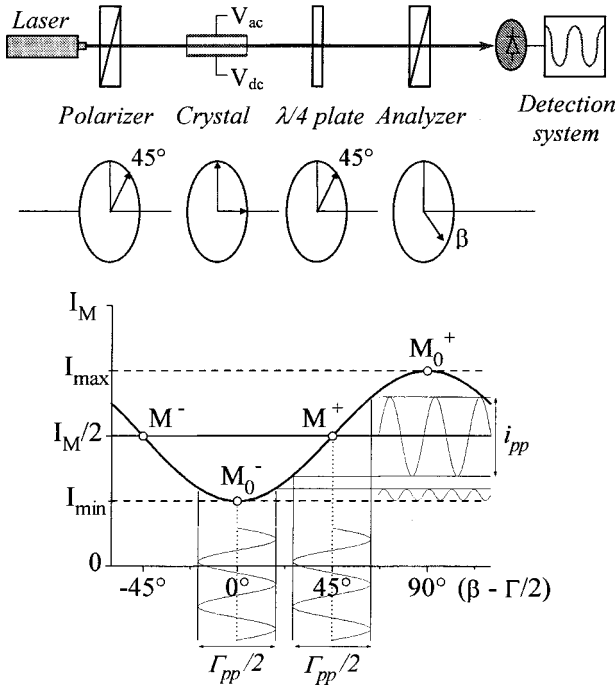


Fig. 4. Sénarmont setup and its transfer function.

is submitted to dc and ac voltages. The field-induced variations of the birefringence are measured for different angular positions of the sample in the cell. Two kinds of measurements are done: dc cycles of the birefringence and frequency dispersions of the effective EO coefficient $n^3 r_{\text{eff}}$.

To record the dc cycle of the birefringence, the output analyzer of the setup is rotated continuously to track the minimum of the light intensity, whereas the bias is varied slowly between -700 V and $+700$ V. A superimposed ac voltage can be used as a probe to obtain and track the double-frequency optical signal at the minimum of light intensity: this improves the accuracy of the recording. The cycling time of the bias is set approximately to one hour. The field-induced birefringence Δn is deduced from the rotation β of the analyzer by the following equation:

$$\Gamma = 2\beta = 2\pi L \times \Delta n / \lambda, \quad (1)$$

where λ is the wavelength in vacuum and Γ is the field-induced phase shift between the two components of the light wave crossing the thickness L of the crystal.

To record the frequency dispersion $n^3 r_{\text{eff}}(\omega)$, the sample is initially brought to the coercive state by a convenient bias, $V_{\text{dc}} = 90$ V (determined from the dielectric measurements; see below). This precaution yields two benefits: (i) the contribution of domain dynamics to EO effect is enhanced; (ii) the possible contributions coming from the coefficients r_{12} , r_{22} , r_{32} , and r_{62} , which are specific for the low-temperature phase, are averaged to zero by the domain structure. Thus the EO effect can be attributed to r_{42} only. The peak-to-peak amplitude V_{pp} is set to 50 V in the frequency range 300 Hz–200 kHz. For each frequency point the effective EO coefficient $n^3 r_{\text{eff}}$ is determined from the peak-to-peak amplitude of the modulated optical signal by the following equation:

$$n^3 r_{\text{eff}} = \frac{2\lambda}{\pi L} \frac{b}{V_{\text{pp}}} \text{Arcsin} \left(\frac{i_{\text{pp}}}{I_{\text{max}} - I_{\text{min}}} \right), \quad (2)$$

where b is the thickness between the electrodes, $(I_{\text{max}} - I_{\text{min}})$ is the full range of the transfer function, and i_{pp} is the average value of the peak-to-peak amplitudes i_{pp}^+ and i_{pp}^- measured at the middle points M^+ and M^- (Fig. 4). As explained in a previous publication,⁵ the double measurement is recommended in the case of RHSe to suppress the contribution of direct intensity modulation owing to the deflection phenomenon. By this procedure the relative error on $n^3 r_{\text{eff}}$ does not exceed 5%, as far as the optical signal largely prevails over the noise. At >200 kHz the optical signal is no longer measurable.

In Eqs. (1) and (2) the thickness L crossed by the light beam through the crystal depends on the propagation direction:

$$L = c / \cos i, \quad (3)$$

where c is the dimension of the sample along the x_3 axis and i is the angle of the wave vector with respect to the x_3 axis inside the crystal. This internal angle is deduced from the angular position i_0 of the rotating holder and corrected for the slight refraction at the interface between the silicon oil and the crystal.

D. Dielectric Measurements

To compare the dispersions of the EO and dielectric responses, the complex permittivity of the crystal is measured with a Sawyer–Tower bridge. At first the influence of the bias is quickly examined in order to find the coercive state, i.e., the value of the dc voltage achieving the maximum of the capacity. The dielectric dispersion is recorded in the same conditions as for the EO measurements ($V_{\text{dc}} = 90$ V and $V_{\text{pp}} = 50$ V from 300 Hz to 500 kHz). The frequency range is extended up to 500 kHz to check that any contribution of domain dynamics vanishes at high frequencies. The typical error on the permittivity is $\pm 5\%$ for the real part ϵ' and $\pm 10\%$ for the imaginary part ϵ'' .

3. RESULTS AND INTERPRETATIONS

A. Birefringence Cycles

Figure 5 shows a typical birefringence cycle recorded at the incidence angle $i = 7.4^\circ$ in the plane (x_2, x_3) . The shape of the loop is similar to the P-E loop and clearly shows the soft ferroelectric behavior of RHSe. The coercive field is ~ 200 V/cm, and the saturation field is ~ 600 V/cm. Similar cycles have been recorded for various incidence angles ranging from -15° to $+15^\circ$. The full range Δn of the cycle is measured for each incidence i and is plotted versus $\sin 2i$ in Fig. 6(a). The linear dependence $\Delta n = f(\sin 2i)$ can be easily understood: as soon as the propagation direction of the light wave is not perpendicular to the domain walls, the birefringences Δn^+ and Δn^- in two neighboring domains are no longer equal, owing to the mutual tilt of the optical indicatrices [Fig. 3(c)]. During dc cycling the birefringence reaches the extreme values Δn^+ and Δn^- corresponding to the single-domain states, provided that the crystal is brought to ferroelectric saturation on both limits of the cycle.

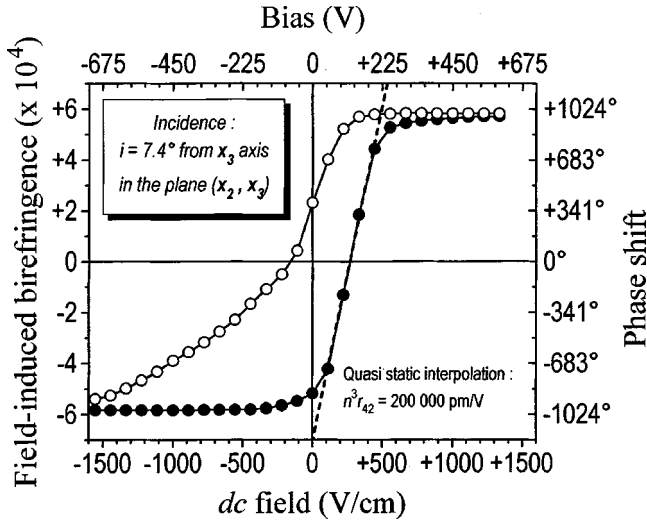


Fig. 5. Typical birefringence cycle recorded versus dc when the direction of propagation is not perpendicular to domain walls. Cycling time is ~ 1 h. The origin of the vertical scale is arbitrarily chosen in order to symmetrize the saturated branches of the loop (i.e., natural birefringence is suppressed).

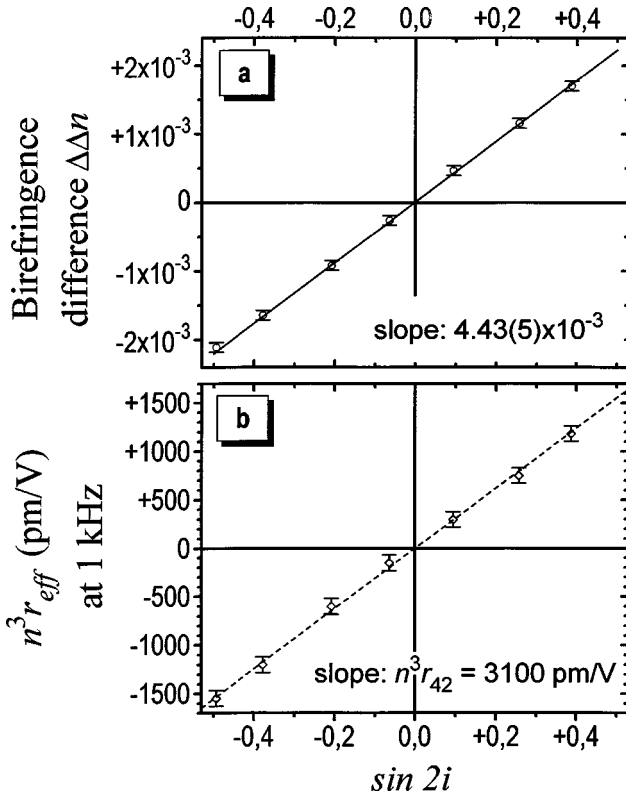


Fig. 6. Variation of (a) the birefringence difference and (b) the effective EO coefficient as a function of the incidence angle i in the plane (x_2, x_3) . $\Delta\Delta n$ is measured on birefringence cycles and corresponds to the full range of the birefringence variation between saturated states. $n^3 r_{\text{eff}}$ is measured at 1 kHz in the coercive state by the classical modulation method under ac amplitude $V_{\text{pp}} = 50$ V ($E_{\text{pp}} \approx 110$ V/cm).

Simple calculations from the laws of crystal optics show that the difference of birefringence between domains can be expressed as

$$\Delta\Delta n = \left(\frac{n_+^2 n_-^2}{n_+ + n_-} \right) \left(\frac{n_2 + n_3}{n_2^2 n_3^2} \right) \Delta n_1 \sin 2\phi_1 \sin 2i, \quad (4)$$

where n^+ and n^- refer to the extraordinary index in neighboring positive and negative domains, respectively [Fig. 3(c)]. For small incidences, n^+ and n^- are nearly constant and approximately equal to n_2 . The pseudo-principal indices, n_j and the pseudoprincipal birefringence Δn_1 of RHSe are known with good accuracy (Table 1). Thus theoretical equation (4) and the experimental plot $\Delta\Delta n = f(\sin 2i)$ can be used to determine the tilt angle ϕ_1 . Linear regression in Fig. 6(a) gives $|\phi_1| = 2.17 \pm 0.03^\circ$. This result is fully consistent with, and more accurate than, the value previously obtained from direct measurement between crossed polarizers⁴ and reported in Table 1.

B. Frequency Dispersions of r_{42} and ϵ

Typical dispersions of the effective EO coefficient are plotted in Fig. 7 for different directions of propagation in the plane (x_2, x_3) . In these plots the sign of $n^3 r_{\text{eff}}$ is meaningful because the phase of the optical signal relative to the ac voltage is taken into account at the middle points of the transfer function. According to the direction of the electric field (nearly parallel to x_2) and to the point group of the polydomain sample (pseudomonoclinic 2), the expression of the effective EO coefficient in the studied configuration is

$$n^3 r_{\text{eff}} = n^3 r_{42} \sin 2i, \quad (5)$$

with $n \approx n_2$ for small incidences. Thus in principle one just has to divide the experimental data $n^3 r_{\text{eff}}(\omega)$ by $n^3 \times \sin 2i$ to obtain the dispersion of r_{42} [Fig. 8(a)]. However, the experimental dispersions recorded at small

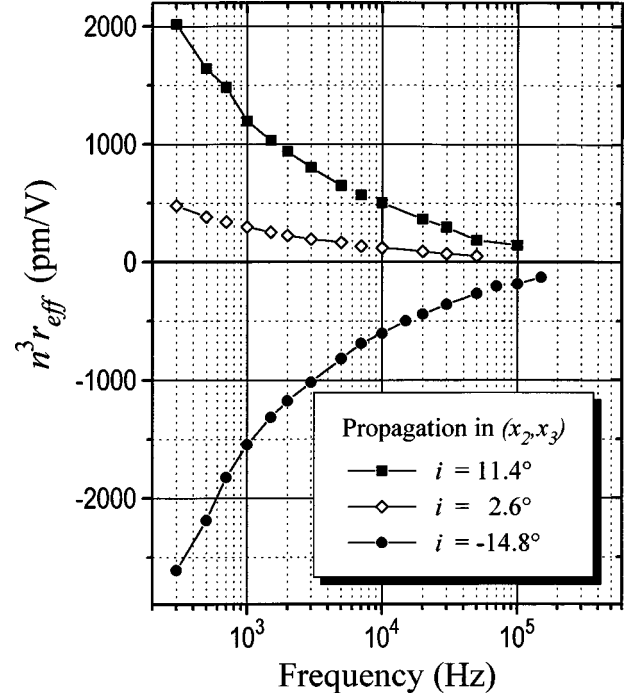


Fig. 7. Frequency dispersion of the effective EO coefficient for three different angles of incidence in the plane (x_2, x_3) . The dotted lines are only to guide the eye.

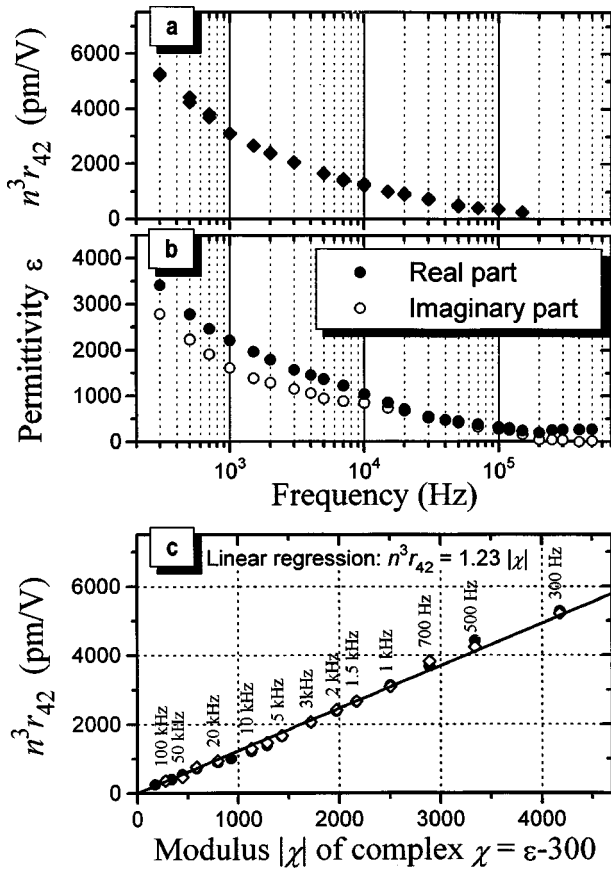


Fig. 8. Correlated dispersions of (a) the dielectric permittivity ϵ and (b) the Pockels coefficient r_{42} . (c) The proportionality between the EO coefficient and the modulus of the complex dielectric susceptibility χ associated with domain dynamics.

incidences ($i < 8^\circ$) should be omitted in this treatment, owing to the large relative error in $\sin 2i$. For better accuracy we prefer plot $n^3 r_{\text{eff}}$ versus $\sin 2i$ at given frequencies and then deduce the corresponding Pockels coefficient r_{42} by a linear regression [Fig. 6(b)].

It is worth noticing that this experimental procedure is particularly suitable to determine EO coefficients belonging to the second half-part of the tensor, with probably higher security and better accuracy than the usual method on samples cut at 45° from the principal axes. Especially in the case of RHSe where r_{42} and r_{52} are both active, our method allows a careful orientation of the pseudoprincipal axes before EO experiments and avoids mixing of the coefficient to be measured. Additionally, for RHSe the measurement at 45° from the axes is very inaccurate because the contrast is poor: it should be necessary to associate two identical samples in series in the laser beam to compensate the walk-off.

The frequency dispersions of r_{42} and ϵ , plotted in Figs. 8(a) and 8(b), are tightly correlated. In the whole frequency range of the measurements, r_{42} is proportional to the modulus of a complex susceptibility, $\chi \approx \epsilon - 300$, as shown in Fig. 8(c). This susceptibility χ clearly corresponds to the contribution of domain dynamics, since at >200 kHz, the real part ϵ' falls to the dc-insensitive value $\epsilon_{\text{HF}} \approx 200$, whereas the imaginary part ϵ'' vanishes.³ The linear regression $r_{42} = f(|\chi|)$ exhibits no break from

300 Hz to 150 kHz: the slope in the medium range 3 kHz–150 kHz is the same as in the low range 300 Hz–3 kHz, where side motion of domain walls has been recently shown by direct experiments under a polarized microscope. This continuity confirms that domain dynamics remains electrically and optically efficient up to 150 kHz in RHSe. Within these experiments it was not possible to measure the Pockels effect accurately at >200 kHz, namely, greater than the frequencies of domain relaxation and piezoelectric resonances. At 200 kHz we observed that the Pockels effect vanishes drastically, together with ϵ'' . We can only conclude that the intrinsic (i.e., ionic and electronic) contributions in the r_{42} coefficient do not exceed 20 pm/V.

We did not measure the other indirect Pockels coefficients. As concerns r_{52} , if we transpose Eq. (4) in the other pseudoprincipal plane, (x_1, x_3) , we obtain immediately the approximate ratio:

$$\frac{r_{52}}{r_{42}} \approx \frac{\Delta n_2 \sin 2\phi_2}{\Delta n_1 \sin 2\phi_1}. \quad (6)$$

From the values of the optical parameters listed in Table 1 we can estimate this ratio to approximately 0.07. Two other indirect coefficients, r_{41} and r_{51} , are authorized by symmetry in the pseudomonoclinic point group 2. But they are probably very small in comparison with r_{42} and r_{52} , respectively, because the polarization vector \mathbf{P}_S of RHSe actually points very close to the b axis (or the x_2 axis).⁶ Correlatively, the permittivity $\epsilon_1 (\approx \epsilon_a)$ is much smaller than $\epsilon_2 (\approx \epsilon_b)$ at low frequency and exhibits practically no domain contribution.

4. USING RHSe IN ELECTRO-OPTIC MODULATORS

Though highly dispersive, the very large EO coefficient of RHSe could allow one to build low-frequency EO modulators with low driving voltages. For instance, at 1 kHz, the value of $n^3 r_{42}$ (3100 pm/V) leads to a reduced half-wave voltage $V_\pi^* = 204$ V at 633 nm, which means that for a crystal of geometrical ratio $L/b = 5$ (for instance, 15 mm/3 mm) the driving voltage at 1 kHz should be 50 V only. At 25 Hz the value of $n^3 r_{42}$ rises to approximately 10 000 pm/V, and in the quasi-static regime ($f < 10^{-3}$ Hz) $n^3 r_{42}$ reaches a tremendous value (200 000 pm/V), as it can be deduced from the slope of the birefringence loop in the linear range (Fig. 5). However, this dc value of $n^3 r_{42}$ is not very meaningful because it is poorly reproducible and it depends on several factors, such as the cycling time, the cutting orientation of the sample, or the quality of the electrodes. For these reasons, and owing to the hysteretic behavior, RHSe should be recommended not for quasi-static applications but rather for low- or medium-frequency application in EO modulation. Additionally, the weak thermo-optic effect of RHSe guarantees a good thermal stability at the working point. However, as for any biaxial crystal operating in a type II configuration (i.e., on a coefficient of the second half-part of the Pockels tensor), RHSe modulators should be built from two identical crystals to achieve compensation of the walk-off and

acceptable contrast. This increases the cost of the cell, but for low-frequency applications this drawback should be largely balanced by the benefit on the power supply, since the half-wave voltage can be reduced to a few ten of volts.

REFERENCES

1. J. P. Salvestrini, M. D. Fontana, M. Aillerie, and Z. Czaplá, "New material with strong electro-optic effect: rubidium hydrogen selenate," *Appl. Phys. Lett.* **64**, 1920–1922 (1994).
2. J. P. Salvestrini, L. Guilbert, M. D. Fontana, and Z. Czaplá, "Electro-optical properties of rubidium hydrogen selenate: influence of the dc electric field and origin of the large electro-optic coefficient," *J. Opt. Soc. Am. B* **14**, 2818–2822 (1997).
3. L. Guilbert, J. P. Salvestrini, M. D. Fontana, and Z. Czaplá, "Correlation between dielectric and electro-optic properties related to domain dynamics in RbHSeO_4 crystals," *Phys. Rev. B* **58**, 2523–2528 (1998).
4. L. Guilbert, J. P. Salvestrini, P. Kolata, F. X. Abrial, M. D. Fontana, and Z. Czaplá, "Optical characteristics of triclinic rubidium hydrogen selenate," *J. Opt. Soc. Am. B* **15**, 1009–1016 (1998).
5. L. Guilbert, J. P. Salvestrini, H. Hassan, and M. D. Fontana, "Combination of phase, intensity and contrast contributions in electro-optic modulation," *IEEE J. Quantum Electron.* **35**, 273–280 (1999).
6. R. Poprawski, J. Mroz, Z. Czaplá, and L. Sobczyk, "Ferroelectrics properties and domain structure in RbHSeO_4 ," *Acta Phys. Pol. A* **55**, 641–645 (1979).